SAND2017-12955C

Validating PMDI-based Polyurethane Foam Models for Fire Safety Applications

Sarah N. Scott[a,b,*], Ryan M. Keedy[a], Victor E. Brunini[a], Matthew W. Kury[a], Amanda B. Dodd[a], James L. Urban[b], A. Carols Fernandez-Pello[b]

[a] *Sandia National Laboratories, 7011 East Avenue, Livermore 94551, USA*
[b] *University of California Berkeley, Department of Mechanical Engineering, Berkeley 94720, USA*

Abstract

Under normal operating conditions, polymer foams protect sensitive items from mechanical, electrical, and thermal shocks. However, in an accident scenario where a fire is present, polymer foams pyrolyze, changing heat paths by creating voids or collecting in new areas. Material properties also change as the virgin material becomes char, gases, and liquids. In a sealed system, the gases created by the pyrolysates can also pressurize the system, leading to breach. Understanding the pyrolysis, heat transfer, and pressurization of these materials in a fire is vital for safety assessments. To investigate such a scenario, a 2-D finite element conduction-radiation model with porous media flow and a pyrolysis chemistry model was created. The gas velocity is solved through Darcys approximation, and the heat transfer and pressurization are determined by solving the continuity, species, and enthalpy equations in the condensed and gas phases. A vapor-liquid equilibrium (VLE) model is used to determine the phase of the pyrolysates. The model was validated using experimental data that showed that the rate of pressurization and the local temperatures are dependent on orientation with respect to gravity. In addition, at the high temperatures and pressures seen in these experiments, it is expected that the organic pyrolysates will exist in both the liquid and gaseous phases. The model reproduces the orientation dependence of the temperature and pressure, as well as the condensation and evaporation of organic pyrolysates. Uncertainty is analyzed using a Latin Hypercube approach, and sensitivities are ranked using the Pearson correlation. The inverted orientation has a larger spread in uncertainty, due the buoyant flow. The model was generally sensitive to the density of the steel, the density of the foam, and the pyrolysis reactions.

Keywords: porous media flow, polyurethane, fire safety, pyrolysis, vapor-liquid equilibrium

*Corresponding author:
Email address: snscott@sandia.gov (Sarah N. Scott)

1. Introduction

Polymer foams are used in any number of applications, from consumer goods, such as couches and automobiles, to protecting items in the storage and shipping. Under normal operating conditions, they provide mechanical, electrical, and thermal isolation, such as in the case with storage and shipping, when polymer foams are used for protection. However, in an accident scenario where a fire is present, polymers are a source of fuel. There are approximately 90,000 accidents involving tractor-trailers in the US per year [1]. In these accidents, the cargo is typically packaged in polymer foams, which can accelerate the spread of a fire through the trailer. The National Fire Protection Association states that there are over a 1,000 warehouse fires in the US per year, and they cite flammable solids, liquids, and gases as the item first ignited in 6% of these fires [2]. In air travel, there are concerns over the shipment of electronics that contain lithium batteries, as they are known to overheat and catch fire [3]. Electronics are often packaged in polymer foams for protection against shocks. In addition, electronics may be placed in a sealed container, to avoid contact with water. However, the gases created by pyrolysis can pressurize a sealed system, leading to an explosion. Understanding how polymer foams behave in a range of scenarios is vital to fire safety analyses.

While modeling polymers and other organics in high heat environments is crucial, it is also challenging due to complex physics, uncertain thermal properties, and the relatively low pyrolysis temperatures. When polymers are exposed to a source of heat, such as fire, they undergo both physical and chemical changes [4]. Not only to the pyrolysates have new material properties, but the heat paths of the system are altered by creating voids or by dripping onto components. The changing heat paths and pressurization can change the outcome of safety assessments.

To successfully model the pyrolysis of polyurethane, a chemical kinetics mechanism must be proposed. This is typically done by performing thermogravimetric analysis combined with Fourier transform infrared spectroscopy (TGA-FTIR) [5, 6]. To successfully simulate the pyrolysis of a solid, more than just the kinetic mechanism must be modeled. Heat, momentum, and mass transfer must also be considered. These simulations have been performed for a variety of materials, from woods and other natural materials [7], to polymers such as PMMA [8], and polyurethanes [9]. Darcys law has been used to numerically study the flame stabilization in a porous burner [10, 11], as well as the flow through a pyrolyzing medium [12, 13]. Darcys law has also been used to study the heat and mass transport in developing char layers in polymers [14].

The liquid phase is also of interest when studying pyrolyzing polymers. For thermoplastics, an external heat source can cause the polymer to melt and flow. Melting polymers can change the flammability properties of the material [15] as well affect the upward flame spread [16]. The melting of the polymers can also cause the dripping and pooling of flammable liquid [17, 18].

One challenge with developing numerical models is determining the material and chemical properties of the materials being modeled. Optimization methods, such as genetic algorithms, shuffled complex evolution, and sequential quadratic programming can be useful in this regard [19–22]. Statistics can be brought to bear not only on model calibration but also model uncertainty [23, 24] and sensitivity [25, 26]. These methods can also be combined to conduct rigorous validation of a model [27, 28], or to understand the probability of an event occurring, for example, power cable failure [29]. While these are all powerful tools, it has been shown that once uncertainty is propagated through a high number of reaction mechanisms, the resulting spread in the simulated data can be larger than when using a smaller number of mechanisms [30, 31].

This work presents a porous media plus Arrhenius-rate based chemistry modeling technique used to describe the pyrolysis, heat transfer, and pressurization of polymeric methylene diisocyanate (PMDI)-polyether-polyol-based polyurethane foam when heated in a sealed container. A vapor-liquid equilibrium (VLE) model is added, as at the temperature and pressures seen within the sealed container, it is possible for the pyrolysates to be in the condensed or vapor phase. The results of the model are compared with experiment. Uncertainty is analyzed, and sensitivities are discussed.

2. Experimental Motivation

Prior experimental work studied PMDI pyrolysis in a configuration consisting of a cylindrical stainless steel container filled with foam along with an embedded metal object (Fig. 1). The temperature of the lid was maintained until the gases generated by the decomposing foam caused the can to breach. Experiments were performed in upright and inverted orientations (Figure 2), and pressure and temperature were monitored. More information about these experiments can be found in [32]. The inverted experiments are shorter in duration than the upright experiments, due to faster pressuriza-

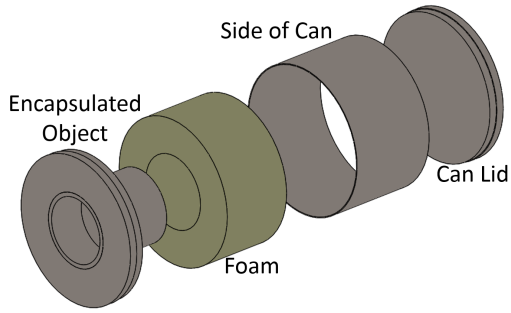

Figure 1: Exploded view of the geometry

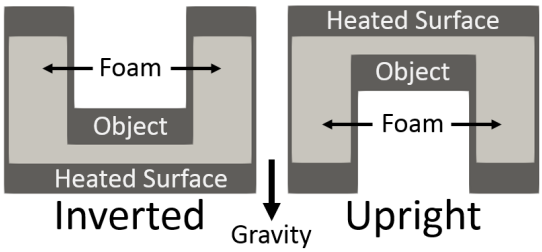

Figure 2: Description of upright and inverted heating, using a 2D representation of the geometry shown in Figure 1, where the can lid is the heated surface.

tion. This difference in response is believed to be caused by the flow of both liquid and gaseous pyrolysates.

3. Computational Model

3.1. Porous Media

The porous media model approach assumes the can is filled with foam that may exist in two phases: the condensed (solid) phase and the gas phase. The condenced phase foam has an associated porosity, which is a function of reaction. In the gas phase, Darcy's law is used to approximate the flow of the fluid and the continuity, species, and enthalpy conservation equations are solved. The ideal gas equation of state is used to relate pressure and density. In the condensed phase, the species and enthalpy equations are solved, and the two phases are coupled through source terms in the species equations and a volumetric heat transfer term in the enthalpy equations. This derivation is based on the model in Lautenberger *et al.* [33].

In this model, the conductivities of the char and virgin foams are determined by summing the volume averaged conductivities for each solid phase. An effective radiative conductivity is then added to this value, based on the diffuse approximation for radiation heat transfer through an optically thick medium. The reaction kinetics were derived through TGA-FTIR [34–36], and approximated by:

Table 1: Major pyrolysis products

Molecule	Formula	Molar Mass (g/mol)
Propylene glycol	$C_3H_8O_2$	76
Aniline	$C_6H_5NH_2$	93
4-methylaniline	C_7H_9N	107
Phenyl isocynatate	C_7H_5NO	119

$$FoamA \rightarrow 0.56CO_2 + 0.44LMWO \quad (1a)$$

$$FoamB \rightarrow HMWO \quad (1b)$$

$$FoamC \rightarrow 0.5char + 0.5HMWO \quad (1c)$$

Where $FoamA$, $FoamB$, and $FoamC$ are representative moieties of PMDI, comprising fractions of 0.45, 0.15 and 0.4, respectively. Low molecular weight organics ($LMWO$) and high molecular weight organics ($HMWO$) represent two general classes of organic molecules with an average weight of 80 and 120 g/mol, respectively. Table 1 shows a list of the major pyrolysates detected through FTIR.

3.2. Vapor-Liquid Equilibrium

The organic products listed in Table 1 have saturation pressures such that they are expected to condense at the pressures and temperatures seen experimentally. Figure 3 shows the quality of aniline, one of the major decomposition products, over the range of pressures and temperatures seen in the experiment. Laid over the quality graph is the experimental response. The since these lines pass through the region where could be in either the gas or liquid phase, it is necessary to include a model to calculate the vapor-liquid split.

To this end, vapor-liquid equilibrium equations were added to the porous media framework. For each species participating in the vapor-liquid equilibrium (CO_2, $HMWO$, $LMWO$) a reaction representing the evaporation and condensation of the species is incorporated in the model:

$$CO_2^{\text{liquid}} \leftrightarrow CO_2^{\text{gas}}$$

$$HMWO^{\text{liquid}} \leftrightarrow HMWO^{\text{gas}}$$

$$LMWO^{\text{liquid}} \leftrightarrow LMWO^{\text{gas}}$$

The rate of each of these reactions is modeled using a form of the Hertz-Knudsen equation [37], modified to allow for non-ideal behavior by using the fugacity of

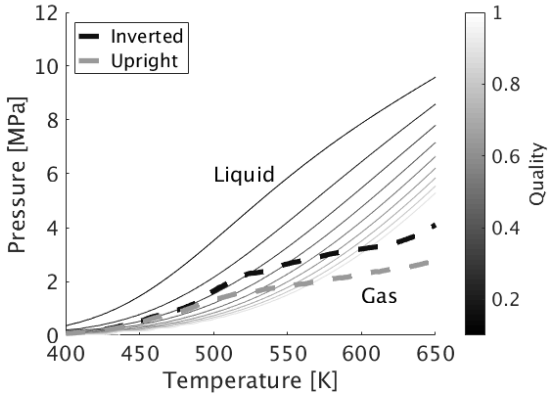

Figure 3: The contour lines show the quality of aniline for the pressures and temperatures seen in the experiment. The dashed lines are the experimental response, which pass through the region where aniline would be in both a liquid and gaseous state.

the species in each phase in place of the pressure and saturation pressure:

$$\omega = \frac{A}{2 - C_c}\left(\frac{2}{\pi MRT}(C_e f_{\text{liquid}} - C_c f_{\text{gas}})\right)^{1/2} \quad (3)$$

where A is the specific surface area, M the molecular weight of the species, C_e and C_c the evaporation and condensation coefficients, and f_{liquid} and f_{gas} the fugacities of the species in each phase respectively. For the purposes of the VLE model we are primarily interested in modeling equilibrium and have no data on the kinetics of the phase change. In these mixtures $C_e = C_c$ and is sufficiently large to maintain equilibrium but not make the kinetics unnecessarily stiff. Each gas-phase species are treated as ideal, so $f_{\text{gas}} = P_i$ where P_i is the partial pressure of the species. The fugacities of the $HMWO$ and $LMWO$ liquid species are modeled using the Antoine equation:

$$\log_{10}\left(f_{\text{liquid}}\right) = A - \frac{B}{T + C} \quad (4)$$

with coefficients based on aniline. Finally, the fugacity of CO_2 in the liquid phase is modeled using Henry's law $f_{\text{liquid}} = H(T)$ since there is interest in regimes above the critical pressure of CO_2.

A 2-D finite element model composed of tetrahedral elements is evaluated in the Sierra Thermal/Fluids multiphysics code [38] to computationally simulate the experiments. Convective and radiative boundary conditions are applied to all sides of the can, with the exception of the heated surface, where a radiative boundary condition is prescribed.

Table 2: Parameters used in LHS method

Foam (virgin, liquid, char)	Bulk Density
	Solid Density
	Rosseland Coefficient
	Bulk Conductivity
	Specific Heat Capacity
	Permeability
	Molecular Weight
Reactions	Heat of Reaction
	Activation Energy
	Mass Fractions
Gas Products	Specific Heat Capacity
	Mass Diffusivity
	Viscosity
	Molecular Weight
	Saturation Pressure
Steel	Density
	Thermal Conductivity
	Specific Heat
	Emissivity
Boundary Conditions	Convection Coefficient
	Lid Temperature

3.3. Model Uncertainty

Model uncertainty and sensitivity are evaluated in Dakota [39] using a Latin Hypercube Sampling (LHS) approach. See Saltelli *et al.* [40] and Helton [41] for a description of the LHS method. The LHS method requires specifying a distribution for each parameter. Because data are not available to formulate a distribution, a functional form is assumed. As a first estimate, a truncated normal distribution for each parameter (Table 2) is assumed with a mean and standard deviation. The mean is assumed to be a value of 1 that is multiplied by the nominal parameter values (*e.g.*, thermal conductivity, $k(T) = p_i k_{nom}(T)$). 420 LHS samples were selected. The parameters were varied by ±10%, except for the lid temperature (±2%), the activation energy (±2%), and the virgin foam density (±5%). The lid temperature and foam density were both reduced because they are well known, and the activation energy was reduced such that it would encompass the experimental TGA data. When a LHS approach is used, correlation coefficients can be directly calculated provided that the number of LHS runs is greater than the number of parameters. The correlation coefficients are computed using the Pearson correlation [32]. This approach assumes a linear correlation between the response and the parameter and is also referred to as the Pearson correlation coefficient.

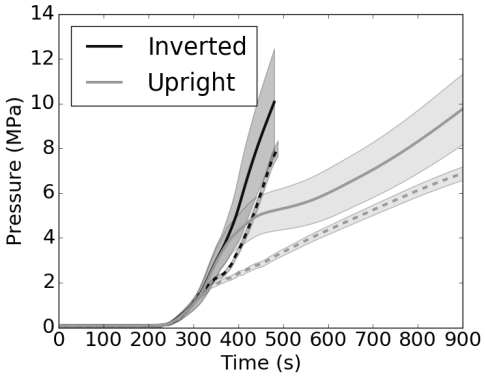

Figure 4: Simulation results (solid) with experimental values (dashed) for upright (grey) and inverted (black) for the pressure in the can. Simulation and experiment are both presented with ±2 standard deviations of the data.

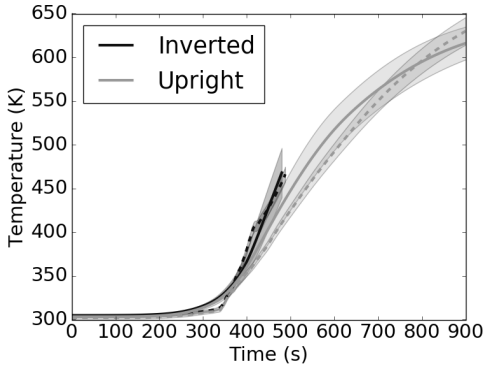

Figure 5: Simulation results (solid) with experimental values (dashed) for upright (grey) and inverted (black) for the temperature of the embedded object. Simulation and experiment are both presented with ±2 standard deviations of the data.

4. Results and Discussion

To validate the model, it is compared to experimental results with a virgin foam density of approximately 320 kg/m^3 (20 lb/ft^3) heated to 1073 K at a rate of 150 K/min. The simulations are terminated when the can in the experiment breached, 480 seconds in the inverted configuration and 900 seconds in the upright. In the experiment, the pressure and the temperature of the object are monitored, so are the quantities used to validate the model. The uncertainty of the model is analyzed by calculating the average and standard deviation of the responses from the ensemble of runs. The average result for pressure, with ±2 standard deviations for both the simulation and experimental error, is presented in Figure 4. While the average pressure is higher than the experiment for both orientations, the qualitative agreement is good. The model is able to predict the differentiation between the orientations, and the shapes of the curves are similar to the experimental results. In the inverted case, the experimental data hits the bottom edge of the bound of uncertainty. The range of the uncertainty at the end of the simulation is 3.3 MPa for upright and 4.8 MPa for inverted. The main contributors to the uncertainty are shown in Table 3, in order of importance based on a response weighted time integration of the Pearson correlation. In general, the pressure was most sensitive to parameters that controlled the CO_2 production. The average result for the temperature of the embedded object, also with ±2 standard deviations for both the simulation and experimental error, is presented in Figure 5. The average result for temperature matches very well with the experimental results. The differentiation between the models is well predicted, and the experiment lays within the bounds of uncertainty for both orientations. The range of the uncertainty at the end of the simulation is 40 K for upright and 60 K for inverted. As seen in Table 3, heat flux and steel density dominate, as is expected since the object is steel, however, the foam properties and reaction mechanisms are in play, as the most direct heat path is through the foam.

Table 3: Top Five Sensitivity Results

	Inverted	**Upright**
Pressure	*FoamA* Mass Fraction	*FoamA* Mass Fraction
	Heat Flux	CO_2 Mass Fraction
	CO_2 Mass Fraction	Steel Density
	Activation Energy *FoamC*	Virgin Foam Bulk Density
	Virgin Foam Bulk Density	Heat Flux
Temperature	Heat Flux	Steel Density
	Steel Density	Heat Flux
	Activation Energy *FoamC*	Virgin Foam Bulk Conductivity
	Char Rosseland Coefficient	Activation Energy *FoamC*
	Foam Specific Heat	Char Rosseland Coefficien

The liquid mass fraction (on a condensed phase basis) is plotted in Figure 6, along with the progression of the reaction (contour lines). The reaction front is not a single line due to the three step reaction. The contour furthest from the heated surface represents the separation between virgin foam and reacted foam. As the *FoamA* reaction has fastest rate, it is the first to be consumed, while *FoamC*, which the slowest rate, is the last. Between the two contour lines is a mixture of reacted and unreacted foam, and between the second contour and the heated surface is char. The reaction creates gasses that are free to flow throughout the foam domain. It is from these gases that the liquid is formed. As seen in Figure 6, when the gases advect to cooler regions of the can, they condense, and form liquid deposits. These deposits can be seen in the virgin foam, as well as on

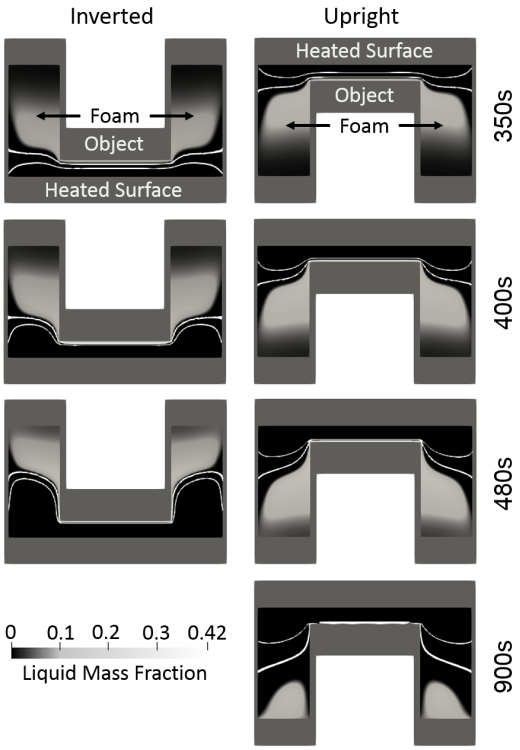

Figure 6: Results of the nominal simulation, where the foam is colored by the liquid mass fraction (on a condensed phase basis), and the progress of the reaction is marked by the contour lines, where the space between the lines is where the reaction is occurring. This is shown for several points in time, notably 480 seconds (when the inverted can breached) and 900 seconds (when the upright can breached). The can remains for reference only.

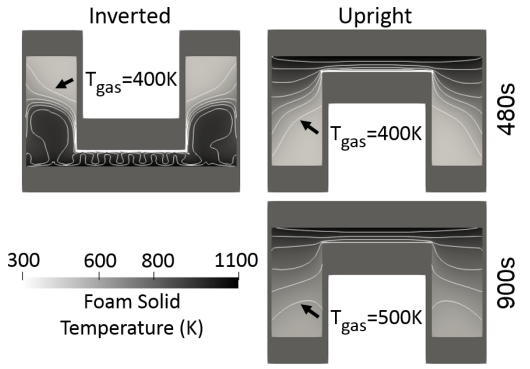

Figure 7: Results of the nominal simulation, where the foam is colored by the solid phase temperature, and the isotherms represent the gas temperature, in increments of 100 K. The temperatures are shown at 480 seconds (when the inverted can breached) and 900 seconds (when the upright can breached. The can remains for reference only.

the object, as it is cooler than the adjacent char. As time progresses, the temperature increases, and not only does the reaction progress, but the liquid product turn into a gas. These are both routes through which the pressure will increase.

In Figures 4 and 5, the temperature and pressure responses of the upright and the inverted do not differentiate themselves until between 350 and 400 seconds. This can also be seen in Figure 6, where the shape of the reaction front and the liquid mass fraction of the foam is very similar at 350 seconds, but by 400 seconds, there is a difference between upright and inverted. From that point, the reaction progresses faster in the inverted than in the upright orientation. At 480 seconds, in the inverted orientation both reaction contour lines are well past the object, whereas in the upright, there is a larger spread between the two lines, and neither has progressed as as far. This can be explained by the difference in the temperatures fields, as shown in Figure 7. Here the foam is colored by the solid phase temperatures, and the contours show the gas phase temperature, in increments of 100 K. In the inverted case, buoyant gas plumes can be seen. These plumes begin to form at 370 seconds, and increase the heat transfer to the virgin foam. The shape of the plumes in Figure 7 and the shape the reaction front in Figure 6 show how this influence the reaction, and thus gas production and pressure rise. Another feature of the inverted to note is the high temperature gradient near the reaction front, as well as a 10-15 K difference between the gas and solid phase temperatures. In the upright, there are no plumes, the temperature gradient is much lower, and the solid and gas phase temperatures tend to be within a couple degrees of each other. The heat is slower to move through the foam domain, which is reflected in the slower progression of the reaction front. However, between 480 seconds and 900 seconds, the can does heat substantially, as can be seen in the evaporation of the liquid products. The reaction front also widens, so while the *FoamA* and *FoamB* reaction continues to progress, increasing the pressure, the production of char slows.

Many of the observations from Figures 6 and 7 bring light to the uncertainty analysis and sensitivity study. For example, the inverted orientation has a larger spread in uncertainty. This is due to the buoyant flow. Small changes to parameters can causes the flow to accelerate or decelerate, changing the rate at which heat is transferred. In the minimum pressure and temperature cases, the buoyant flow appears nearly a minute later than in the maximum pressure and temperature cases. The flow can be effected by any number of parameters,

such as the heat flux, the amount of gas produced, and the progress of the reaction. For example, when the activation energy of $FoamC$ reaction is lowered, char is more easily produced. This would be true in both the upright and inverted, but inverted is more sensitive to the response because the char is more permeable than the virgin foam, thus the flow can move faster.

5. Conclusions

The safety analysis of engineered systems that use polymer foams is dependent on accurate modeling the pyrolysis, heat transfer, and in the case of sealed systems, pressurization. To that end, a model was created to simulate pyrolyzing PMDI polyurethane foam in a pressurizing sealed system. The model is able to simulate orientation-dependent pressure and temperature responses. The results compare well in both temperature and pressure. The uncertainty is analyzed and sensitivities were assessed using a strategy where the uncertainty in the input parameters is (mostly) equal across the parameter space. It was seen that the inverted orientation is more sensitive to variation in the parameters, due to the effect on the buoyant flow, which is the main driver of heat in that orientation.

This work is a step forward in modeling the pyrolysis of polymers with products in the liquid phase. In the future, now that a liquid phase can be generated, a model to advect that liquid needs to be implemented. In addition, the sensitivity of the model to the production of CO_2 highlights the need for a reexamination of the reaction scheme. The reactions are known to be dependent on pressure, as seen in the difference between the unconfined and partially confined TGA results [36]. However, the pressures reached using partially confined TGA pale in comparison to the pressures seen within the can. Future work should incorporate a pressure dependent reaction mechanism.

Acknowledgments

Sandia National Laboratories is a multimission laboratory managed and operated by National Technology and Engineering Solutions of Sandia, LLC., a wholly owned subsidiary of Honeywell International, Inc., for the U.S. Department of Energys National Nuclear Security Administration under contract DE-NA0003525. SAND2017-12662 C

References

[1] Large truck and bus crash facts 2015 (Mar 2017).
URL https://www.fmcsa.dot.gov/safety/data-and-statistics/large-

[2] R. Campell, Structure fires in warehouse properties, Tech. rep., National Fire Protection Angency (2015).

[3] Faa urges airlines to assess lithium battery risks (Feb 2016).
URL https://www.faa.gov/news/updates/?newsId=84785

[4] C. Beyler, M. Hirschler, Thermal Decomposition of Polymers, in: SFPE Handbook of Fire Protection Engineering, National Fire Protection Association, 2001, pp. 110–131.

[5] T. Rogaume, L. B. Valencia, E. Guillaume, F. Richard, J. Luche, G. Rein, J. L. Torero, Development of the Thermal Decomposition Mechanism of Polyether Polyurethane Foam Using Both Condensed and Gas-Phase Release Data, Combustion Science and Technology 183 (7) (2011) 627–644.

[6] L. Bustamante Valencia, T. Rogaume, E. Guillaume, G. Rein, J. L. Torero, Analysis of principal gas products during combustion of polyether polyurethane foam at different irradiance levels, Fire Safety Journal 44 (7) (2009) 933–940.

[7] C. D. Blasi, Analysis of Convection and Secondary Reaction Effects Within Porous Solid Fuels Undergoing Pyrolysis, Combustion Science and Technology 90 (5) (1993) 315–340.

[8] I. Vermesi, N. Roenner, P. Pironi, R. M. Hadden, G. Rein, Pyrolysis and ignition of a polymer by transient irradiation, Combustion and Flame 163 (2016) 31–41.

[9] O. M. Putzeys, A. C. Fernandez-Pello, G. Rein, D. L. Urban, The piloted transition to flaming in smoldering fire retarded and non-fire retarded polyurethane foam, Fire and Materials 32 (8) (2008) 485–499.

[10] A. J. Barra, J. L. Ellzey, Heat recirculation and heat transfer in porous burners, Combustion and Flame 137 (1-2) (2004) 230–241.

[11] A. J. Barra, G. Diepvens, J. L. Ellzey, M. R. Henneke, Numerical study of the effects of material properties on flame stabilization in a porous burner, Combustion and Flame 134 (4) (2003) 369–379.

[12] A. Dodd, C. Lautenberger, A. Fernandez-Pello, Numerical examination of two-dimensional smolder structure in polyurethane foam, Proceedings of the Combustion Institute 32 (2) (2009) 2497–2504.

[13] A. B. Dodd, C. Lautenberger, C. Fernandez-Pello, Computational modeling of smolder combustion and spontaneous transition to flaming, Combustion and Flame 159 (1) (2012) 448–461.

[14] J. Staggs, Heat and mass transport in developing chars, Polymer Degradation and Stability 82 (2) (2003) 297–307.

[15] C. Denecker, J. J. Liggat, C. E. Snape, Relationship between the thermal degradation chemistry and flammability of commercial flexible polyurethane foams, Journal of Applied Polymer Science 100 (4) (2006) 3024–3033.

[16] J. Zhang, T. Shields, G. Silcock, Effect of melting behaviour on flame spread of thermoplastics, Fire and Materials 21 (1).

[17] K. M. Butler, A model of melting and dripping thermoplastic objects in fire, Fire and materials (2009) 341–352.

[18] K. M. Butler, E. Oate, S. R. Idelsohn, R. Rossi, Modeling polymer melt flow using the particle finite element method, in: Eleventh International Interflam Conference, London, England, 2007, pp. 929–940.

[19] G. Rein, C. Lautenberger, A. Fernandez-Pello, J. Torero, D. Urban, Application of genetic algorithms and thermogravimetry to determine the kinetics of polyurethane foam in smoldering combustion, Combustion and Flame 146 (1-2) (2006) 95–108.

[20] M. Bruns, J. Koo, O. Ezekoye, Population-based models of thermoplastic degradation: Using optimization to determine model

parameters, Polymer Degradation and Stability 94 (6) (2009) 1013–1022.
[21] S. Garcia, J. Guynn, E. P. Scott, Use of Genetic Algorithms In Thermal Property Estimation: Part Ii - Simultaneous Estimation Of Thermal Properties, Numerical Heat Transfer, Part A: Applications 33 (2) (1998) 149–168.
[22] M. Chaos, M. M. Khan, N. Krishnamoorthy, J. L. de Ris, S. B. Dorofeev, Evaluation of optimization schemes and determination of solid fuel properties for CFD fire models using bench-scale pyrolysis tests, Proceedings of the Combustion Institute 33 (2) (2011) 2599–2606.
[23] K. J. Overholt, O. A. Ezekoye, Quantitative testing of fire scenario hypotheses: a bayesian inference approach, Fire Technology 51 (2) (2015) 335–367.
[24] M. C. Bruns, Inferring and Propagating Kinetic Parameter Uncertainty for Condensed Phase Burning Models, Fire Technology 52 (1) (2016) 93–120.
[25] S. I. Stoliarov, N. Safronava, R. E. Lyon, The effect of variation in polymer properties on the rate of burning, Fire and Materials 33 (6) (2009) 257–271.
[26] G. T. Linteris, Numerical simulations of polymer pyrolysis rate: Effect of property variations, Fire and Materials 35 (7) (2011) 463–480.
[27] P. Summers, B. Lattimer, S. Case, S. Feih, Predicting compression failure of composite laminates in fire, Composites Part A: Applied Science and Manufacturing 43 (5) (2012) 773–782.
[28] P. Summers, B. Lattimer, S. Case, S. Feih, Sensitivity of thermo-structural model for composite laminates in fire, Composites Part A: Applied Science and Manufacturing 43 (5) (2012) 783–792.
[29] A. Matala, S. Hostikka, Probabilistic simulations of cable fires in a cable tunnel, in: 20th international conference on structural mechanics in reactor technology, Helsinki, Finland, 2009.
[30] N. Bal, G. Rein, On the effect of inverse modelling and compensation effects in computational pyrolysis for fire scenarios, Fire Safety Journal 72 (2015) 68–76.
[31] N. Bal, G. Rein, Relevant model complexity for non-charring polymer pyrolysis, Fire Safety Journal 61 (2013) 36–44.
[32] S. N. Scott, A. B. Dodd, M. E. Larsen, J. M. Suo-Anttila, K. L. Erickson, Validation of heat transfer, thermal decomposition, and container pressurization of polyurethane foam using mean value and latin hypercube sampling approaches, Fire Technology 52 (1) (2016) 121–147.
[33] C. Lautenberger, C. Fernandez-Pello, Generalized pyrolysis model for combustible solids, Fire Safety Journal 44 (6) (2009) 819–839.
[34] K. Erickson, A. Dodd, R. Hogan, K. J. Dowding, Heat Transfer, Foam Decomposition, and Container Pressurization: Comparison of Experimental and Modeling Results, Interscience Communications Ltd, Nottingham, UK, 2010.
[35] K. L. Erickson, A. Dodd, E. Quintana, Physical Behavior and Container Pressurization During Thermal Decomposition of Polyurethane Foams, in: Proceedings of BCC 2011, Stamford, 2011.
[36] K. L. Erickson, Thermal decomposition mechanisms common to polyurethane, epoxy, poly (diallyl phthalate), polycarbonate and poly (phenylene sulfide), Journal of Thermal Analysis and Calorimetry 89 (2) (2007) 427–440.
[37] M. Knudsen, The kinetic theory of gases: some modern aspects.
[38] Sierra Core Team, Sierra Thermal Fluids Code (2017).
[39] Dakota Core Team, Dakota, A Multilevel Parallel Object-Oriented Framework for Design Optimization, Parameter Estimation, Uncertainty Quantification, and Sensitivity Analysis: Version 6.0 Users Manual, SAND2014-4633 (Jul. 2014).
[40] A. Saltelli, K. Chan, E. Scott, Chapter 6, in: Sensitivity analysis, Wiley, New York.
[41] J. Helton, Latin hypercube sampling and the propagation of uncertainty in analyses of complex systems, Tech. Rep. SAND2001-0417, Sandia National Laboratories, Albuquerque (2001).